DTU Library

# Automatic Triple Phase Shift Modulation for DAB Converter with Minimized Power Loss

**Lin, Fanfan; Zhang, Xin ; Li, Xinze ; Sun, Changjiang ; Cai, Wenjian ; Zhang, Zhe**

*Published in:*
IEEE Transactions on Industry Applications

*Link to article, DOI:*
10.1109/TIA.2021.3136501

*Publication date:*
2022

*Document Version*
Peer reviewed version

# Automatic Triple Phase Shift Modulation for DAB Converter with Minimized Power Loss

Fanfan Lin, *Student Member*, *IEEE*, Xin Zhang, *Senior Member*, *IEEE*, Xinze Li, *Student Member*, *IEEE*, Changjiang Sun, *Member*, *IEEE*, Wenjian Cai, *Member*, *IEEE*, Zhe Zhang, *Senior Member*, *IEEE*

***Abstract*—Currently, triple phase shift (TPS) modulation has attracted more and more attention of researchers as an advanced modulation strategy for dual active bridge converter (DAB). Since it has three degrees of freedom, it can realize better performance both in soft switching ranges and power efficiency. However, how to choose these three degrees of freedom to realize optimal power efficiency of DAB converter becomes a concern for researchers. Generally, there exist two difficulties to apply efficiency-oriented TPS modulation. The first difficulty lies in the analysis process in which the main task is to figure out the relationships between modulation parameters and power loss. The three modulation parameters in TPS bring difficulties in analysis and deduction process, which suffers from high computational burden and low accuracy. Additionally, the second difficulty lies in the real-time realization of TPS modulation. If a look-up table is applied to store the optimized modulation parameters, it is highly likely that its discrete nature will result in unsatisfactory modulation performance. Therefore, this paper proposes an efficiency-oriented automatic TPS (ATPS) modulation approach which utilizes neural network, particle swarm optimization and fuzzy inference system respectively in its three stages. The proposed ATPS is able to mitigate labor in computational burden with a highly automatic fashion. Finally, this proposed ATPS has been validated with 1kW hardware experiments.**

***Index Terms*—Dual active bridge, triple phase shift, power loss, neural network, particle swarm optimization, fuzzy inference system.**

## I. Introduction

Dual active bridge (DAB) converter was proposed in 1992 which has two full bridges as connected by a high-frequency transformer [1]. Since then, it has attracted more and more attention because it enjoys many advantages including bidirectional power transfer capability, high power density and galvanic isolation [2], [3]. It has wide applications, such as solid state transformer [4], uninterrupted power supply [5], energy management system [6] and DC microgrid [7]. The typical schematic of DAB converter is shown as the following Fig. 1.

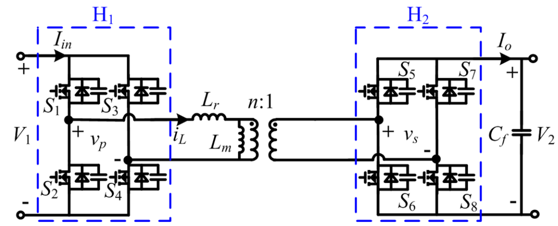

Fig. 1. Typical circuit structure of DAB converter: full bridges $H_1$, $H_2$ and a galvanic-isolated transformer with single $L$.

To achieve better operating performance of DAB converter, modulation strategy for it has been a hot research topic. Phase shift strategy for full bridges is a popular modulation strategy for its easy implementation. Generally, it includes three main modulation strategies: single phase shift (SPS), dual phase shift (DPS) and triple phase shift (TPS). With SPS strategy, the phase shift between the full bridges $H_1$ and $H_2$ can be modulated [8]. DPS has one more modulation parameter compared with SPS, which is the duty ratio of the full bridges [9]. Compared with SPS and DPS, TPS enjoys better modulation performance because it enjoys three degrees of freedom, which are the duty ratio of full bridge $H_1$, the duty ratio of full bridge $H_2$ and the phase shift between them [10], [11]. TPS is worth investigation not only because it has wider zero voltage switching (ZVS) range and lower power loss [12], [13], but also because it is the general version for SPS and DPS.

When TPS is adopted, how to choose three modulation parameters becomes a concern for researchers and engineers. Usually power efficiency, as a performance indicator, needs to be considered when modulation parameters are optimized because that DAB converter is expected to have as less power loss as possible to save energy [14]–[16]. In order to optimize modulation parameters for better power efficiency, the relationships between modulation parameters and power loss should be figured out. However, three degrees of freedom of TPS result in severe difficulties in the analysis of power loss. In general, there are two different ways to analyze power loss: piecewise model [12], [14], [17]–[19] and harmonic analysis [11], [15], [20]–[22]. In the first method, waveforms are analyzed piece by piece based on different mode boundaries. This method needs hard work for its high complexity [14]. In the second method, generalized harmonics model is built with Fourier series transformation on the primary and secondary voltages. Only fundamental component of harmonic model is used for analysis as approximation [11]. In this way, analytical complexity can be relieved, but the accuracy of results is undermined. In a word, the existing methods for analyzing the power loss under TPS fail to achieve simplicity and satisfactory accuracy at the same time.

Manuscript received April 27, 2021; revised Jun 22, 2021; revised October 02, 2021; accepted December 01, 2021. This work was supported by Start-up grant of Professor Zhang at Zhejiang University. (*Corresponding author: Xin Zhang*).

Fanfan Lin is with ERI@N, Interdisciplinary Graduate Program, Nanyang Technological University, Singapore 639798, Singapore. (e-mail: fanfan001@e.ntu.edu.sg).

Xin Zhang is with the College of Electrical Engineering, Zhejiang University, Hangzhou 310027, China, and with Hangzhou Global Scientific and Technological Innovation Center, Zhejiang University, Hangzhou 310058, China. (e-mail: zhangxin_ieee@163.com).

Xinze Li and Wenjian Cai are with the School of Electrical and Electronic Engineering, Nanyang Technological University, Singapore 639798, Singapore. (e-mail: xinze001@e.ntu.edu.sg; ewjcai@ntu.edu.sg).

Changjiang Sun is with Rolls-Royce@NTU Corporate Lab, Nanyang Technological University, Singapore 639798, Singapore. (e-mail: changjiang.sun@ntu.edu.sg).

Zhe Zhang are with the Department of Electrical Engineering, Technical University of Denmark, Kgs. Lyngby 2800, Denmark. (e-mail: zz@elektro.dtu.dk).

After choosing the values of three modulation parameters, how to realize TPS in real-time implementation is another important concern. There exist two commonly used methods: formula calculation and look-up table application. In formula calculation method [23]–[25], the formula derived by analysis process will be saved in the controller. However, as discussed above, the analytical formula suffers either from high complexity or low accuracy. As for the second method in which the optimized modulation parameters are saved in a look-up table [15], [26], [27], the discrete nature of look-up table may result in a situation when optimal modulation parameters cannot be found for a specific experimental condition. Thus, how to realize TPS in real-time implementation with simplicity and accuracy is also worth investigating.

In recent years, attention of researchers in power electronics has been attracted by artificial intelligence (AI) techniques. Some researchers are making attempts to apply AI tools to solve problems in TPS modulation to achieve optimal performances for DAB converters. To simplify the optimization of modulation parameters, the authors of [27] applied Q-learning to solve the optimization problem and then saved the optimal results in a look-up table. This approach can improve optimization accuracy, but it still suffers from complicated and inaccurate analysis as well as discrete modulation results. Beside the application of AI in optimization, attempts have been tried to adopt neural network (NN) in the realization of TPS modulation [28]. If operating parameters are given to a trained NN, the corresponding optimal modulation parameters will be outputted. However, this approach still needs complex analysis process for the training of NN and its modulation performance can be further improved because of the open-loop control.

Targeted at the difficulties both in the analysis and realization process as discussed above, this paper proposes an efficiency-oriented automatic TPS (ATPS) modulation approach based on AI tools. In this approach, there are three main stages, and each stage applies an AI tool. In the first stage, NN is applied to learn the relationships between modulation parameters and power loss, to substitute the traditional analysis process. In the second stage, particle swarm optimization (PSO) algorithms are utilized to search for the best modulation parameters for the sake of minimum power loss. In the last stage, fuzzy inference system (FIS) has been adopted to realize TPS in real-time implementation, achieving continuous modulation results. With these three stages, efficiency-oriented TPS modulation can be carried out in a highly automatic fashion, contributing to less working burden for engineers.

The organization of the rest of this paper is summarized as the following. In Section II, the introduction to TPS operating principles and descriptions for the existing problems are provided. After that, elaboration of the proposed ATPS will be given in details in Section III. In Section IV, applicational design cases are provided. Afterwards, the results of hardware experiments are displayed to verify the effectiveness of the proposed ATPS approach in Section V. In the last section, conclusion for this paper is drawn.

## II. TPS Operating Principles and Problem Descriptions

### *A. Preliminaries: TPS Operating Principles*

As shown in Fig.1, full bridges of the DAB converter $H_1$ and $H_2$ are connected with an isolated high-frequency transformer with a single $L$. The ac voltages generated by the two full bridges are $v_p$ and $v_s$.

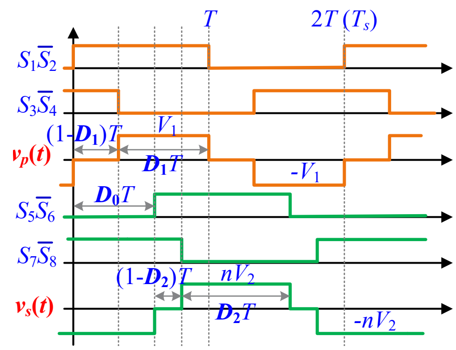


Fig. 2. Modulation waveforms of TPS modulation.

Fig. 2 describes the operation principle of TPS scheme with the gate-drive waveforms $S_1$ to $S_8$, $v_p$ and $v_s$. $T$ is half of the switching cycle. $D_1$ is the duty ratio of the first full bridge $H_1$ whose range is $0 \le D_1 \le 1$. $D_2$ is the duty ratio of the second full bridge $H_2$ whose range is $0 \le D_2 \le 1$. And $D_0$ is the phase difference between them and usually the range of it is $-1 \le D_0 \le 1$. By tuning these three degrees of freedom, the current through inductor $L$ and the transferred power $P_{out}$ can be adjusted. The expression of the maximum transferred power ($P_{out\_max}$) is given in (1) [27], in which $f_s$ is the switching frequency. With $P_{out\_max}$, the limit for inductor $L$ can be also calculated, as expressed in (2).

$$P_{out\_\max} = \frac{nV_1V_2}{8f_sL} \tag{1}$$

$$L \le \frac{nV_1V_2}{8f_sP_{out\_\max}} \tag{2}$$

### *B. Existing Problems in the TPS Modulation with Minimized Power Loss*

Generally, the procedure of efficiency-oriented TPS modulation can be divided into three stages: analysis stage, optimization stage and realization stage, as shown in Fig. 3.

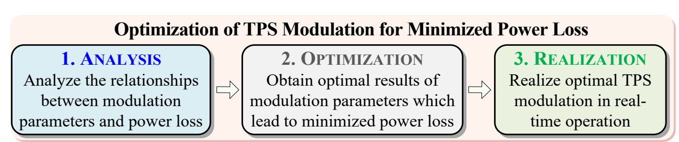


Fig. 3. Three stages in achieving optimal TPS scheme with minimized power loss.

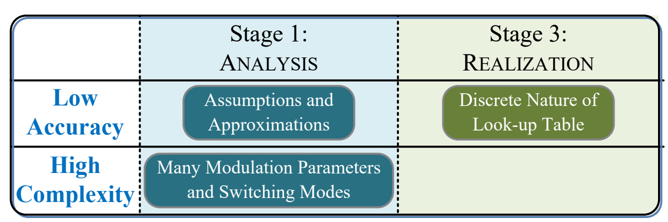


Fig. 4. Existing problems in the TPS modulation with minimized power loss.

In the first stage, main task is to analyze the relationships between modulation parameters ($D_0$, $D_1$, $D_2$) and power loss $P_{loss}$.

This article has been accepted for publication in a future issue of this journal, but has not been fully edited. Content may change prior to final publication. Citation information: DOI 10.1109/TIA.2021.3136501, IEEE Transactions on Industry Applications



When the operating parameters (output power $P_{out}$ and $V_2$) have been decided, how the choices of modulation parameters affect the power loss should be figured out. Afterwards, for different operating parameters, the modulation parameters will be optimized to achieve optimal power efficiency. Finally, in realization stage, efficiency-oriented optimal modulation parameters will be applied in real-time situations based on practical operating parameters.

Whereas there are some difficulties in the analysis stage and realization stage which will lead to highly complex, error-prone and inaccurate results.

(*a*) *Problem in Stage* 1*: Deduction and Analysis of Power Loss*

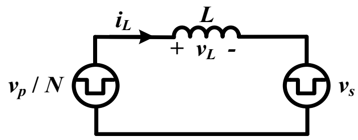


Fig. 5. Switching model of DAB with a single inductor $L$.

In existing research works, main power loss of the TPS-modulated DAB converter can be divided into conduction loss, copper loss, core loss and switching loss [29]. The detailed analysis will be conducted by two different methods: piecewise model and harmonic analysis.

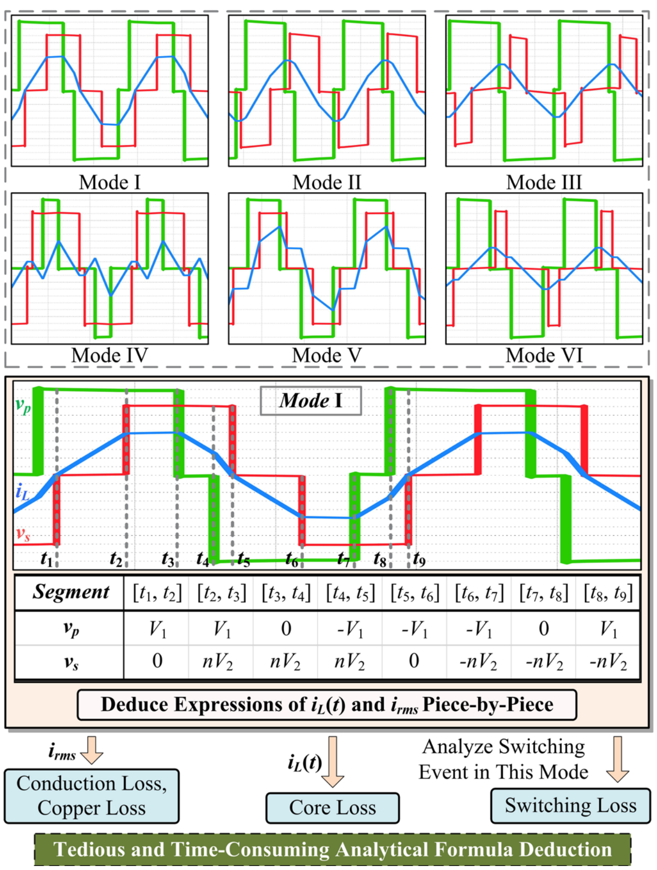


Fig. 6. Problem in piecewise model: complex piece-by-piece analysis of total power loss for all six operating modes (Mode I to Mode VI) of TPS scheme.

In the piecewise model, the operating modes of TPS modulation, which totally have 6 modes [23], will be analyzed one by one by using the switching model of DAB in Fig. 5. In every mode, $i_L(t)$ should be analyzed piece by piece within a switching cycle by using the inductor volt-second balance principle [25], [30]. Calculation of $i_{rms}$ is even more complex, since it requires the integration of the squares of $i_L(t)$. This deduction and analysis process is described with Fig. 6. This method requires a lot of time-consuming works with complicated computation.

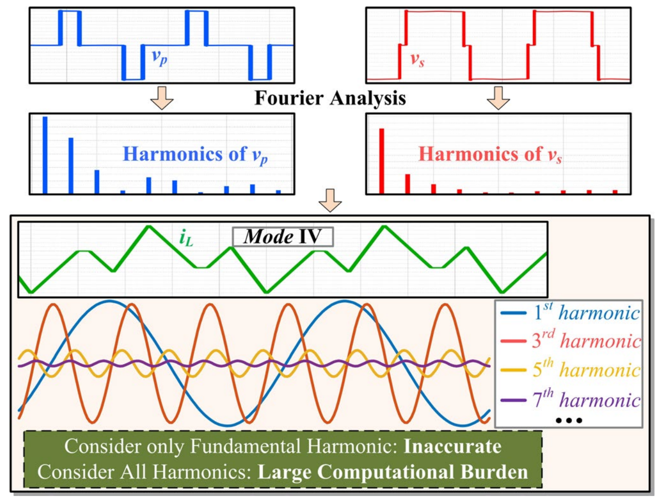


Fig. 7. Problems in harmonic model.

In the harmonic analysis method [20] shown in Fig. 7, Fourier series transformation will be applied to $v_p$ and $v_s$, with which the instantaneous and rms current can be derived. This method only considers the fundamental components of the harmonic model as an approximation for all practical purposes, which can simplify the calculation, but it deteriorates accuracy. If all the harmonics (infinite possibilities) are considered, the computational burden will be unacceptable.

(*b*) *Problem in Stage* 3: *Realization of TPS Modulation*

After searching for the optimal modulation parameters in Stage 2, the common way for realizing TPS modulation is to save the optimization results in a look-up table. This look-up table is stored in the hard disk of microcontroller. As for online real-time experiments, after the operating parameters are detected, corresponding modulation parameters will be searched for throughout the look-up table and then be executed [15].

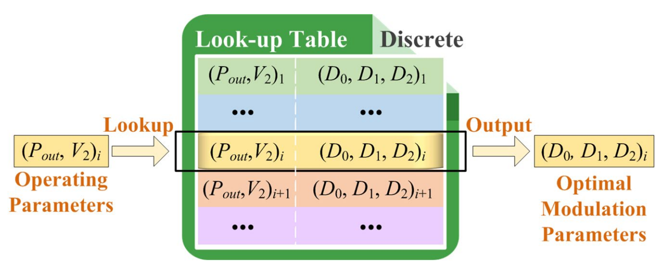


Fig. 8. Problem in the realization of TPS: discreteness of look-up table for the real-time implementation of TPS modulation.

What should be emphasized is the discrete nature of the look-up table, which leads to incomplete information about modulation as presented in Fig. 8. Chances are that some specific operating parameters cannot be found in this look-up table. In this case, usually, the most similar operating parameters will be taken as approximation [27]. However, this will sacrifice the modulation performance definitely.

To conclude, there are two main problems in the analysis stage and realization stage of efficiency-oriented TPS modulation that need to be dealt with, otherwise high analytical complexity and low modulation accuracy will be unacceptable.

## III. The Proposed Automatic TPS Modulation

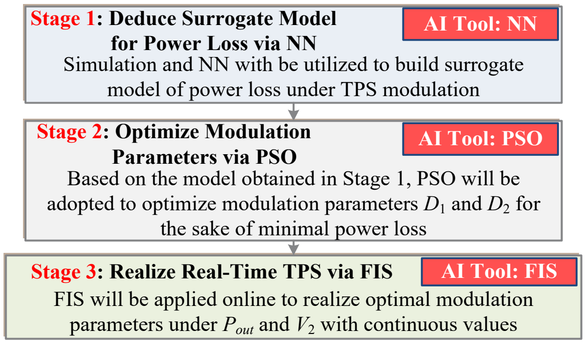


Fig. 9. Three stages of the proposed ATPS.

Targeted at the problems mentioned above, in this paper, an automatic TPS (ATPS) optimization approach to realize minimal power loss under fluctuating operating parameters has been proposed. The proposed ATPS as shown in Fig. 9 incorporates three stages, deduce surrogate model for power loss via NN, optimize modulation parameters via PSO, and realize real-time TPS via FIS.

### A. Stage 1: *Deduce Surrogate Model for Power Loss via NN*

To relieve the heavy deduction burden of engineers, a powerful regression AI technique, NN, is automatically trained with the data from simulation in Stage 1, serving as a surrogate model for power loss. The NN-based surrogate model can be regarded as the equivalent data-driven model for power loss. Hence, Stage 1 automates the analysis of power loss under TPS, the flowchart of which is shown in Fig. 10.

Stage 1 consists of three steps as follows. Before Stage 1, the design conditions such as output power $P_{out}$, switching frequency $f_s$, and input $V_1$ and output voltages $V_2$ should be specified.

First of all, to decide the combinations of operation parameters ($P_{out}$, $V_2$) and modulation parameters ($D_1$, $D_2$) for conducting simulation and training NN, $P_{out}$, $V_2$, $D_1$ and $D_2$ are evenly selected within the ranges [$P_{out\_min}$, $P_{out\_max}$], [$V_{2\_min}$, $V_{2\_max}$], [0, 1], and [0, 1], respectively. Assume $N_1$, $N_2$, $N_3$ and $N_4$ number of values are evenly selected for $P_{out}$, $V_2$, $D_1$ and $D_2$ within their ranges, respectively, so the number of parameter combinations in total is $N_1 \times N_2 \times N_3 \times N_4$. The reason why the values of $P_{out}$, $V_2$, $D_1$, $D_2$ are evenly selected is that: with uniform and complete data distributions, NN can achieve the best prediction accuracy.

Secondly, simulation is built using PLECS, which can simulate all kinds of power losses, including conduction loss, switching loss, copper loss and core loss [31]. For all the chosen $N_1 \times N_2 \times N_3 \times N_4$ combinations of $P_{out}$, $V_2$, $D_1$, $D_2$, this PLECS model will run to gather performance data for total power loss. To automatically control and run the PLECS model, some programming languages such as python should be used to interact with PLECS software.

After that, with the total loss data generated by simulation, NN is properly trained, whose inputs are operating parameters and modulation parameters $P_{out}$, $V_2$, $D_1$, $D_2$, and output is the total power loss performance $P_{loss}$. The automatically trained NN can be regarded as a data-driven surrogate model for power loss, based on which the power loss performance of any valid possible values of $P_{out}$, $V_2$, $D_1$, $D_2$ can be evaluated.

With Stage 1 discussed above, the model for total power loss under TPS modulation can be automatically deduced, and no mathematical expressions are required in this process, freeing engineers from time-consuming and complex manual deduction.

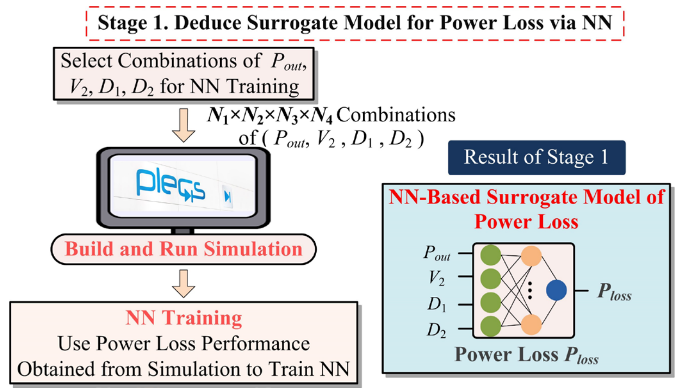


Fig. 10. Flowchart of Stage 1: deduce surrogate model for power loss via NN.

### B. Stage 2: *Optimize Modulation Parameters via PSO*

Stage 2 searches for the optimal modulation parameters $D_1$ and $D_2$ under selected operating parameters $P_{out}$ and $V_2$ by interacting with the NN-based surrogate model of power loss as resulted from Stage 1. The optimization problem of efficiency-oriented TPS modulation can be formularized as follows.

**Under selected $P_{out}$ and $V_2$, the objective is:**

$$P_{loss}^{*} = \min_{D_1, D_2} P_{loss}(D_1, D_2, P_{out}, V_2) \tag{3}$$

**Subject to:**

$$0 \le D_1 \le 1 \tag{4}$$

$$0 \le D_2 \le 1 \tag{5}$$

In this paper, to realize the closed-loop control of TPS, $D_0$ is adjusted by the output of PI controller. As a result, the modulation parameters considered in (3) are $D_1$ and $D_2$.

To solve the TPS optimization in (3) to (5), PSO algorithm, a population-based evolutionary algorithm, is adopted for its good global searching capability and fast convergence speed in continuous optimization problems [32]. PSO algorithm imitates the social and individual behavior of birds to find the global optimum. And the dynamic equations are shown in (6) and (7), in which $X$ is the particle's position representing the modulation parameters ($D_1$, $D_2$), and $V$ is the change of position. Through iterating over (6) and (7), the optimal $D_1$ and $D_2$ to realize minimized power loss for given $P_{out}$ and $V_2$ will be found.

$$V_i^{m+1} = \omega V_i^m + c_1 r_1 (Pbest_i^m - X_i^m) + c_2 r_2 (Gbest^m - X_i^m) \tag{6}$$

$$X_i^{m+1} = X_i^m + V_i^m \tag{7}$$

In (6) and (7), $m$ represents the $m^{th}$ iteration. *Pbest* and *Gbest* are the personally best information and the globally best information, respectively. $c_1$ and $c_2$ are the acceleration factors,

This article has been accepted for publication in a future issue of this journal, but has not been fully edited. Content may change prior to final publication. Citation information: DOI 10.1109/TIA.2021.3136501, IEEE Transactions on Industry Applications



the values of which are 2.05 and 2.05. $\omega$ is the velocity inertia, which linearly decreases from 0.9 to 0.4 in the evolution process of PSO [33].

The detailed flowchart of Stage 2 is shown in Fig. 11. In the beginning, the operating parameters $P_{out}$ and $V_2$ are specified. Before entering the iterations of PSO, the basic parameters will be initialized. And then the position $X$ will be iteratively updated based on (6) and (7). When the stopping criterion is satisfied, the minimal $P_{loss}^*$ found and the optimal $D_1^*$ and $D_2^*$ for the selected $P_{out}$, $V_2$ are stored. The same process repeats for all the considered combinations of $P_{out}$ and $V_2$.

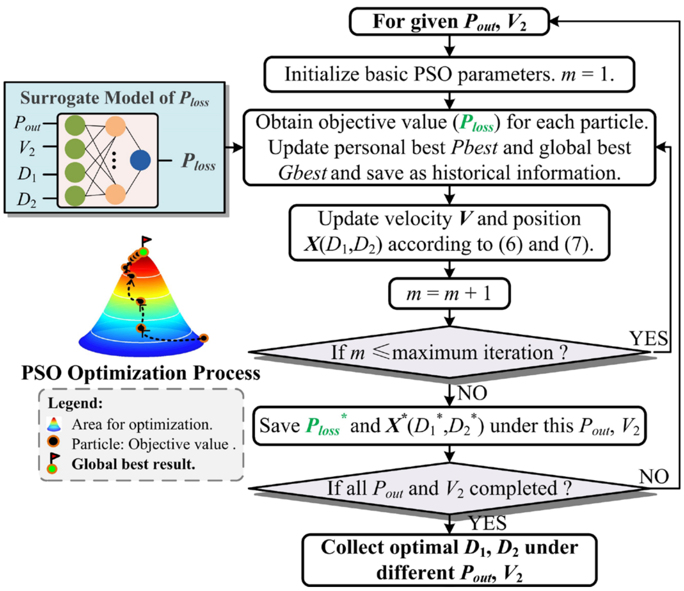


Fig. 11. Detailed flowchart of Stage 2: optimized TPS modulation under given combinations of $P_{out}$ and $V_2$ using PSO algorithm.

In conclusion, Stage 2 of the proposed ATPS adopts PSO algorithm in finding the efficiency-oriented optimal $D_1$, $D_2$ for the selected combinations of operating $P_{out}$ and $V_2$.

### C. Stage 3: *Realize Real-Time TPS with FIS*

In Stage 3 of the proposed ATPS, to mitigate the inaccurate modulation results suffered from the discrete nature of look-up table, this paper utilizes fuzzy inference system (FIS), which can realize real-time TPS modulation given that the operating parameters $P_{out}$ and $V_2$ are continuous. Fig. 12 shows the proposed FIS-based TPS modulation diagram.

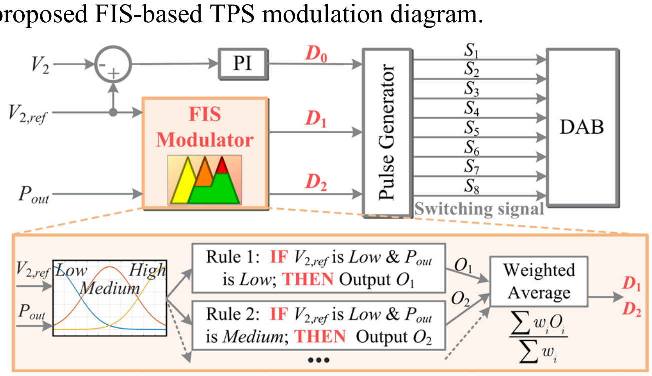


Fig. 12. Stage 3: real-time implementation of optimal TPS scheme via FIS.

To control the output voltage $V_2$ to follow the required reference value $V_{2,ref}$, PI controller should output one of the three modulating parameters ($D_0$, $D_1$, $D_2$). For example, as shown in Fig. 12, $D_0$ is selected to be adjusted by the PI controller, whose input is the difference between $V_{2,ref}$ and the instant value of $V_2$. And the values of $D_1$ and $D_2$ are determined by the FIS modulator, which takes $V_{2,ref}$ and $P_{out}$ as the inputs to achieve optimal TPS modulation under varying operating parameters.

The computational flow of FIS modulator as shown in Fig. 12 is discussed as follows. Firstly, $V_{2,ref}$ and $P_{out}$ will be inputted, and membership functions with different semantic meaning (e.g., $V_{2,ref}$ is high, $P_{out}$ is medium) will compute the membership degree each input belongs to. Subsequently, outputs $O_1$, … $O_N$ will be evaluated by all $N$ fuzzy rules. In the end, the required optimal $D_1$, $D_2$ for the chosen $V_{2,ref}$ and $P_{out}$ are calculated by $O_1$, … $O_N$, with the weight $\omega_i$ for output $O_i$ as evaluated by the activating strength of rules [34].

Via the proposed FIS-based TPS diagram shown in Fig. 12, the inaccurate problem of look-up tables due to its discrete nature is largely mitigated. The proposed diagram can be deployed in online real-time applications to achieve optimal $D_1$ and $D_2$ under continuous $P_{out}$ and $V_2$.

To conclude, in Stage 1 of the proposed ATPS, NN-based surrogate model of power loss is automatically deduced, which significantly reduces the time-consuming manual deduction of analytical formula. Under the selected combinations of operating parameters $P_{out}$ and $V_2$, Stage 2 adopts PSO algorithm to minimize the total power loss. In Stage 3, the proposed FIS-based TPS modulation diagram realizes the real-time implementation under fluctuating operating parameters.

## IV. Application Case by Following the Proposed ATPS

By following the proposed ATPS approach in Section III, an efficiency-oriented optimal TPS scheme for DAB is given. The application case is elaborated below in details.

Table I lists the specifications of the application case, in which the rated power is 1000 W, input and output voltages are 200 V, switching frequency is 20 $k$Hz. The variation ranges of $P_{out}$ and $V_2$ are [100 W, 1000 W] and [160 V, 230 V].

TABLE I. Experimental Specifications

| | | | |
|---|---|---|---|
| **Rated Conditions** | | | |
| $P_{out}$ | 1000 W | $V_1$ | 200 V |
| $V_2$ | 200 V | $f_s$ | 20 $k$Hz |
| **Switching Device** | | | |
| Series | C2M0080120D, Cree | Dead time | 500 $ns$ |
| $R_{DS(on)}$ | 80 $m\Omega$ | $V_{DSS}$ | 1.2 $k$V |
| **Isolated Transformer** | | | |
| Inductor $L$ | 140 $\mu$H | | |
| Core material | Nanocrystalline of iron alloy | | |
| **Limits of $D_1$ and $D_2$** | | | |
| $D_1$ | $D_{1\_min} = 0$; $D_{1\_max} = 1$ | | |
| $D_2$ | $D_{2\_min} = 0$; $D_{2\_max} = 1$ | | |
| **Limits of $P_{out}$ and $V_2$** | | | |
| $P_{out}$ | $P_{out\_min} = 100$ W; $P_{out\_max} = 1000$ W | | |
| $V_2$ | $V_{2\_min} = 160$ V; $V_{2\_max} = 230$ V | | |

### A. Stage 1: *Deduce Surrogate Model for Power Loss via NN*

With the flowchart in Fig. 10, surrogate model of total power loss is automatically deduced via NN.

- Firstly, for complete coverage of the input ranges, each of the $D_1$, $D_2$, $P_{out}$, $V_2$ has been sampled uniformly for 20 points. Hence, total 160000 (20×20×20×20) combinations of $D_1$, $D_2$,

This article has been accepted for publication in a future issue of this journal, but has not been fully edited. Content may change prior to final publication. Citation information: DOI 10.1109/TIA.2021.3136501, IEEE Transactions on Industry Applications



$P_{out}$, $V_2$ have been generated.

- Afterwards, the sampled 160000 combinations of $D_1$, $D_2$, $P_{out}$, $V_2$ are implemented in the built PLECS model to obtain the corresponding total power loss performance $P_{loss}$.
- Stage 3 trains NN according to the total power loss data from simulation, serving as the surrogate model for total power loss. Its inputs are operating parameters $P_{out}$, $V_2$ and modulation parameters $D_1$, $D_2$, and the output is $P_{loss}$. The computational graph of selected NN is shown in Fig. 13, whose structure is listed in Table II. In terms of the root mean square error (RMSE), the selected NN reaches the least error on all the datasets compared with three regression algorithms [35].

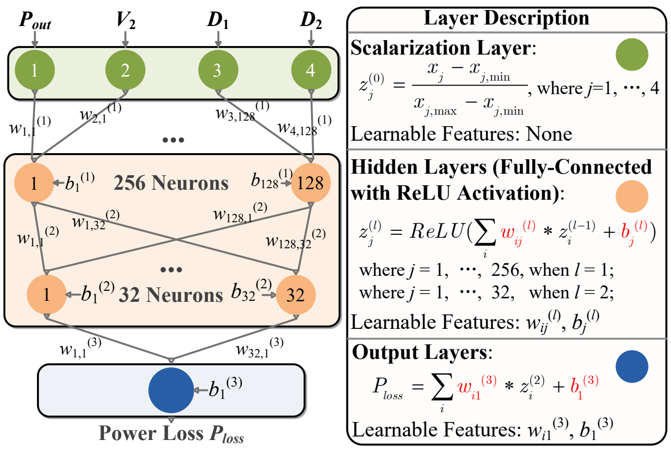

Fig. 13. Computational flow of the adopted NN.

TABLE II. SETTINGS OF THE SELECTED NN AND THE OPTIMIZER

| | |
|---|---|
| **Structure of the Selected NN** | |
| Inputs | Parameters $D_1$, $D_2$, $P_{out}$, $V_2$ |
| Output | Power loss $P_{loss}$ |
| Hidden layer | 2 layers, one has 256 and another has 64 neurons with ReLU function |
| **Optimizer Settings** | |
| Learning algorithm | Adam algorithm [36] |
| Learning factor | 0.0005 |
| Regularization factor | 5e-5 |
| Total iterations | 20000 |

TABLE III. ROOT MEAN SQUARE ERROR OF THE TRAINED NN AND OTHER COMPARED ALGORITHMS

| Error | Training Set | Validating Set | Testing Set |
|---|---|---|---|
| Response Surface | 1.3508 | 1.4734 | 1.4695 |
| Bayesian Regression | 1.3037 | 1.3223 | 1.3066 |
| Support Vector Regression | 0.5007 | 0.5811 | 0.4612 |
| **NN** | **0.1249** | **0.1046** | **0.1341** |

## B. *Stage 2: Optimize Modulation Parameters via PSO*

TABLE IV. SETTINGS OF PSO IN STAGE 2

| Hyperparameter Name | Hyperparameter Value |
|---|---|
| Population size | 30 |
| Maximum iterations | 200 |
| $\omega$: velocity inertia | Linearly decreasing from 0.9 to 0.4 |
| $c_1$, $c_2$: acceleration factors | $c_1$ = 2.05; $c_2$ = 2.05 |

Under the selected operating parameters $P_{out}$ and $V_2$, Stage 2 applies PSO algorithm with the settings in Table IV to interact with the trained NN to search for the optimal $D_1$ and $D_2$. The results of the optimal $D_1$ and $D_2$ in achieving minimal power loss under different operating parameters are given in Fig. 14.

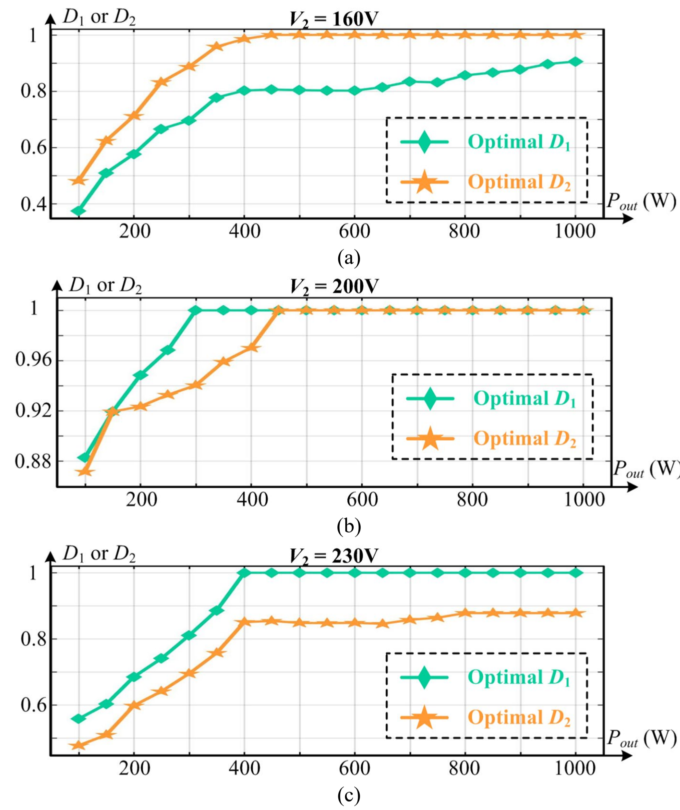

Fig. 14. Optimized modulation parameters $D_1$, $D_2$ versus $P_{out}$ for selected values of $V_2$: (a) $V_2$=160 V; (b) $V_2$=200 V; (c) $V_2$=230 V.

## C. *Stage 3: Realize Real-Time TPS with FIS*

TABLE V. SETTINGS OF FIS

| | |
|---|---|
| Inputs | $P_{out}$, $V_2$ of continuous values |
| Output | Optimal $D_1$, $D_2$ |
| Type of FIS | Type-1 Takagi-Sugeno [33] |
| Membership functions of input | Gaussian, 5 linguistic sets |
| Number of rules | 25 |

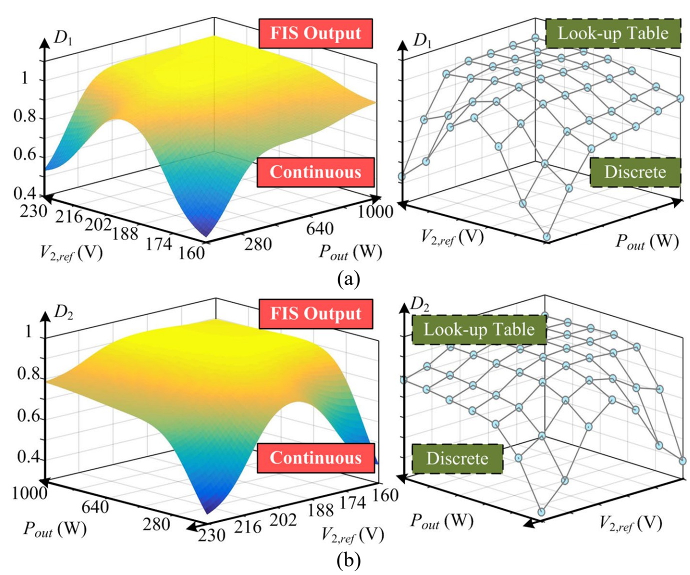

Fig. 15. Modulation surface of FIS regarding $P_{out}$ and $V_2$: (a) modulation surface of $D_1$; (b) modulation surface of $D_2$.

In Stage 3, with the optimal values of $D_1$, $D_2$ under selected operating parameters searched by PSO algorithm, FIS is trained

This article has been accepted for publication in a future issue of this journal, but has not been fully edited. Content may change prior to final publication. Citation information: DOI 10.1109/TIA.2021.3136501, IEEE Transactions on Industry Applications



to realize online continuous modulation. The FIS-based TPS modulation diagram in Fig. 12 enables the real-time operation to achieve minimal power loss under fluctuating operating parameters with continuous values. In this application case, the settings of FIS are listed in Table V. The input memberships are Gaussian type [34] and incorporate five semantic sets (very low, low, medium, high, very high), and the outputs are the optimal $D_1$ and $D_2$. The results of FIS are shown in Fig. 15, the right-side of which shows the discrete values stored in look-up tables. According to Fig. 15, compared with the discrete look-up tables, the proposed FIS-based diagram in Stage 3 is continuous modulation, which can be applied in real-time situations to handle fluctuating $P_{out}$ and $V_2$ with continuous values.

### D. *Computation Complexity to Implement ATPS*

To shed lights on the computation complexity of using the proposed ATPS approach in the application case, the mean processing time of CPU in Stage 1 and 2 is recorded. Besides, in Stage 3, the space and time complexity of FIS-based modulator as respectively reflected by storage size and turnaround time are recorded.

As shown in Table VI, in the computational platform of Intel Xeon CPU with series E5-1630, Stage 1 and Stage 2 of ATPS takes 3.9 days and 2.74 hours to complete, respectively. In the controller platform of Dspace1202 MicroLabBox, the deployed FIS-based modulator achieves 7.53 $\mu$s turnaround time in average, indicating low time complexity, and it only takes up 9.92 $k$B in storage, verifying small space complexity.

TABLE VI. COMPUTATION COMPLEXITY TO IMPLEMENT THE PROPOSED ATPS

| Stages | Offline or Online | Platform | Performance |
|---|---|---|---|
| Stage 1 | Offline | Intel Xeon CPU with series E5-1630, RAM of 16GB | Mean CPU Time: 3.88 days |
| Stage 2 | Offline | | Mean CPU Time: 2.74 hours |
| Stage 3 | Online | Dspace1202 MicroLabBox | Mean Turnaround Time: 7.53 $\mu$s Memory Size: 9.92 $k$B |

## V. EXPERIMENTAL VERIFICATION

To validate the application case in Section IV via the proposed ATPS, hardware experiments have been conducted. The experimental operating details are listed in Table I, and the prototype to conduct hardware experiments is given in Fig.16. The directions of all the waveforms and their notations in the following figures are shown in Fig. 1.

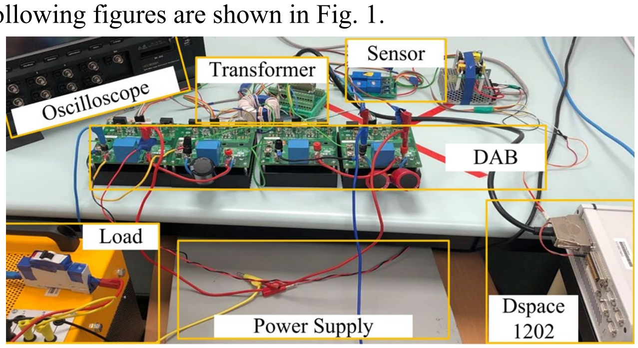


Fig. 16. Prototype platforms in the hardware experiments.

### A. *Waveforms under Rated Operations*

Under rated conditions, DAB operates with the efficiency-oriented optimal $D_1$ and $D_2$ as designed by ATPS, the waveforms of which are shown in Fig. 17. As shown in Fig. 15, the designed efficiency-oriented optimized $D_1$, $D_2$ under rated conditions are equal to 1, so the modulation waveforms ($v_p$, $v_s$) of two full bridges are basically square waves.

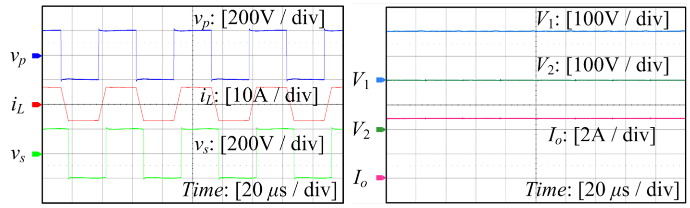


(a) (b)

Fig. 17. Rated operation under $P_{out}$ of 1000 W and $V_2$ of 200 V: (a) modulation waveforms $v_p$, $i_L$ and $v_s$; (b) operating waveforms $V_1$, $V_2$ and $I_o$.

### B. *Waveforms for Selected $P_{out}$ and $V_2$*

Except for the rated operation, the experiments under other $P_{out}$ (900 W, 400 W, 100 W) and $V_2$ (200 V, 160 V, 230 V) are also carried out.

By comparing the modulation waveforms in Fig. 18 with those in Fig. 6, the operating modes of the three experiments in which $V_2$ is 200 V and $P_{out}$ is 900 W, 400 W and 100W are Mode I, Mode I and Mode V, respectively.

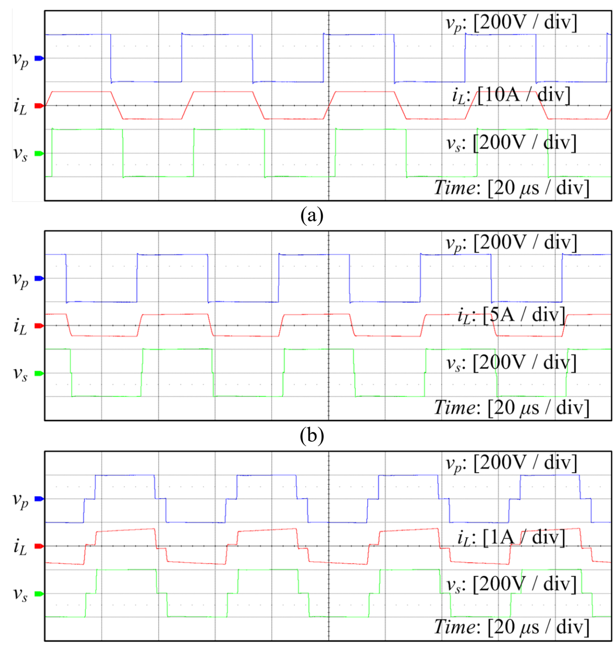


Fig. 18. Modulation waveforms given that $V_2$ is 200V when $P_{out}$ is: (a) 900 W; (b) 400 W; (c) 100 W.

As displayed in Fig. 19, the operating modes of the experiments under $P_{out}$ of 900 W, 400 W and 100 W given that $V_2$ is 160 V are Mode I, Mode I and Mode IV, respectively.

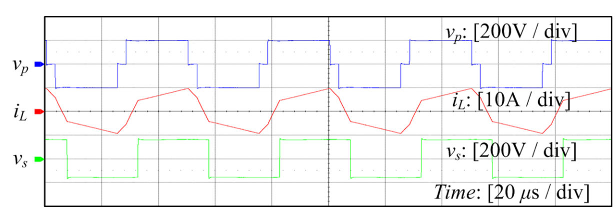


(a)

This article has been accepted for publication in a future issue of this journal, but has not been fully edited. Content may change prior to final publication. Citation information: DOI 10.1109/TIA.2021.3136501, IEEE Transactions on Industry Applications



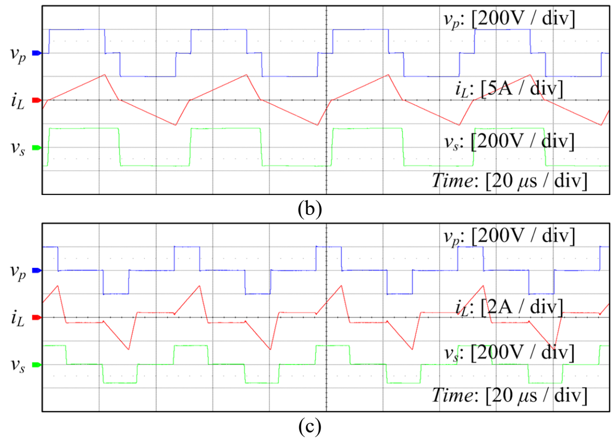


Fig. 19. Modulation waveforms given that $V_2$ is 160 V when $P_{out}$ is: (a) 900 W; (b) 400 W; (c) 100 W.

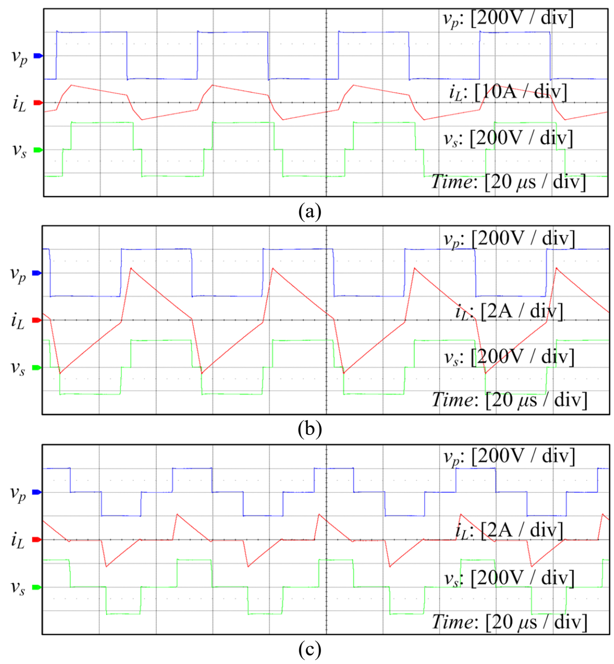


Fig. 20. Modulation waveforms given that $V_2$ is 230 V when $P_{out}$ is: (a) 900 W; (b) 400 W; (c) 100 W.

As shown in Fig. 20, the operating modes of the experiments under $P_{out}$ of 900 W, 400 W and 100 W given that $V_2$ is 230 V are Mode I, Mode V and Mode V, respectively.

### *C. Real-Time Operation under Power and Voltage Step*

While the operating parameters $P_{out}$ and $V_2$ change, optimized $D_1$, $D_2$ are accordingly adjusted via the proposed FIS-based modulator in Fig. 12. The experiments of $P_{out}$ steps and $V_2$ steps as the following validate the real-time implementation.

In the dynamic responses shown in Fig. 21 to 23, the figures in the top show the operating waveforms ($I_o$, $V_1$, $V_2$), while ones in the bottom show the enlarged view of modulation waveforms ($i_L$, $v_p$, $v_s$) at zone1 and zone2.

Firstly, as shown in Fig. 21, by fixing the load resistance at 40 Ω, $V_2$ changes from 200 V to 160 V and steps back from 160 V to 200 V, in which $P_{out}$ is 1000 W at 200 V and 640 W at 160 V.

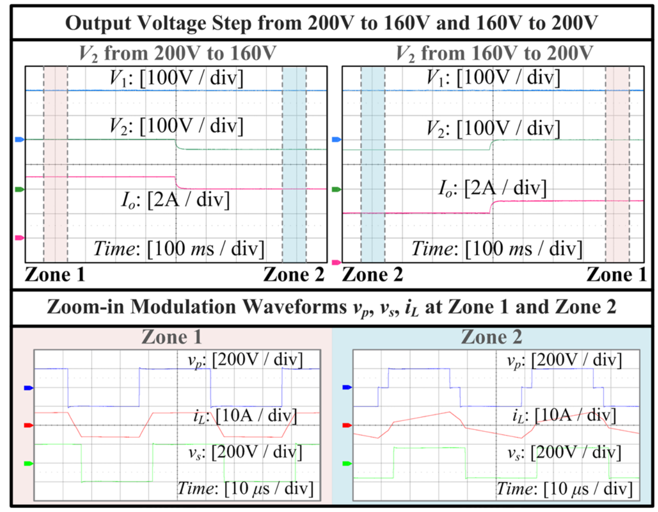


Fig. 21. Waveforms when $V_2$ steps from 200 V to 160 V and from 160 V to 200 V: operating waveforms ($I_o$, $V_1$, $V_2$) during voltage step (top); enlarged modulation waveforms ($i_L$, $v_p$, $v_s$) at Zone1 and Zone2 (bottom).

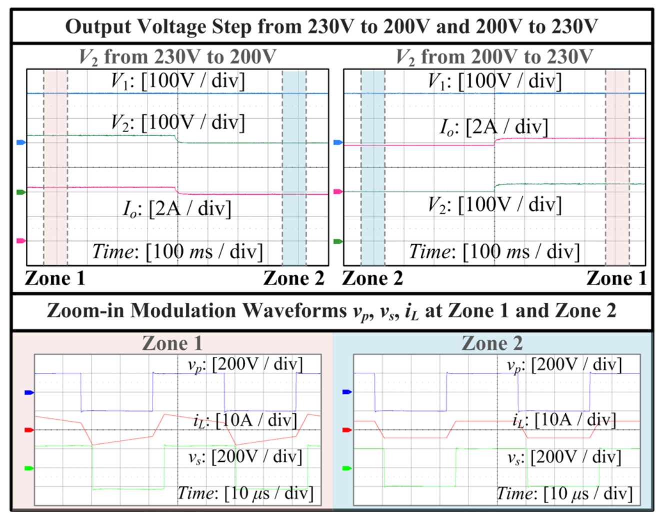


Fig. 22. Waveforms when $V_2$ steps from 230 V to 200 V and from 200 V to 230 V: operating waveforms during voltage step (top); enlarged modulation waveforms at Zone1 and Zone2 (bottom).

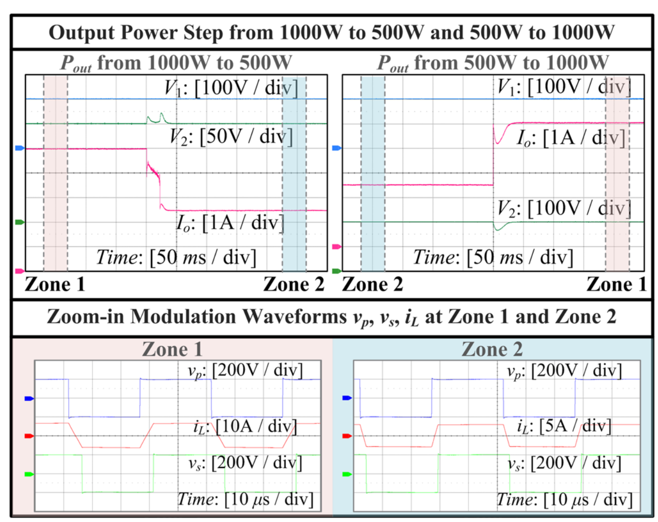


Fig. 23. Waveforms when output power $P_{out}$ steps from 1000 W to 500 W and from 500 W to 1000 W: operating waveforms during voltage step (top); enlarged modulation waveforms at Zone1 and Zone2 (bottom).

Secondly, as presented in Fig. 22, by fixing the load resistance at 52.9 Ω, $V_2$ changes from 230 V to 200 V and steps back from 200 V to 230 V, where $P_{out}$ is 1000 W at 230 V and 756 W at 200 V.

As displayed in both Fig. 21 and 22, while $P_{out}$ and $V_2$ fluctuate, the optimal TPS modulation diagram via FIS can adjust the optimized $D_1$, $D_2$ online to realize minimized power loss, verifying the performance of the FIS modulator in Fig. 12 in real-time scenarios.

Moreover, according to Fig. 23, by keeping $V_2$ fixed at 200 V, the output power $P_{out}$ changes from full load 1000 W to half load 500 W, and steps back from 500 W to 1000 W. According to Fig. 23, when the output power step happens, the output voltage $V_2$ can track the reference value $V_{2,ref}$, validating the closed-loop TPS modulation.

In summary, with the experiments of voltage and power steps, the real-time operating capability of the proposed diagram in Fig. 12 has been validated.

### *D. Efficiency and Peak Current of the Efficiency-Oriented Optimal TPS Modulation with ATPS*

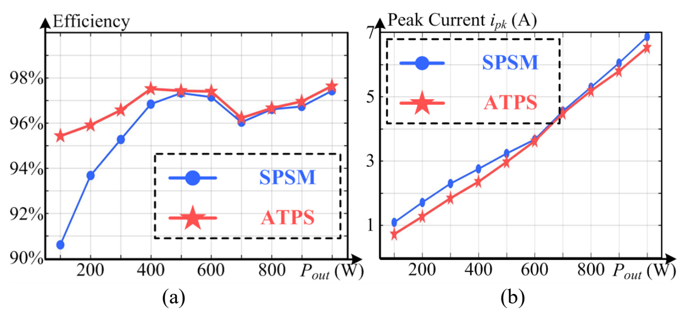


Fig. 24. $\eta$ and $i_{pk}$ of the proposed ATPS compared with SPS modulation given that $V_2$ is 200 V: (a) efficiency $\eta$; (b) current stress $i_{pk}$.

With the proposed ATPS, the optimal TPS modulation in the application case can achieve optimal efficiency performance. Apart from the optimal efficiency performance, the current stress performance (as reflected by the peak current through inductor $i_{pk}$) is also satisfactory. To prove its superior efficiency $\eta$ and current stress $i_{pk}$ performance, standard SPS is compared with. The experimental results of ATPS and SPS under $V_2$ of 200 V, 160 V and 230 V are shown in Fig. 24 to Fig. 26, where the output power is between 100 W and 1000 W.

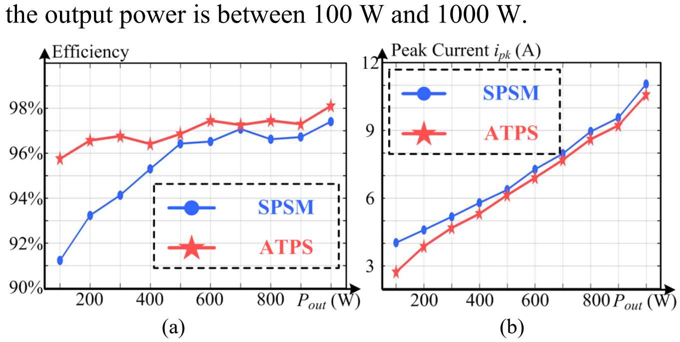


Fig. 25. $\eta$ and $i_{pk}$ of the proposed ATPS compared with SPS modulation given that $V_2$ is 160 V: (a) efficiency $\eta$; (b) current stress $i_{pk}$.

Based on Fig. 24 to Fig. 26, when $P_{out}$ is high, the difference between the optimal TPS and the conventional SPS on the efficiency $\eta$ and current stress $i_{pk}$ performance is trivial. This is because that under high-power conditions, the optimal $D_1$ and $D_2$ as shown in Fig. 15 are close to 1, indicating that the gate-drive control signals of TPS and SPS are approximately the same. When $P_{out}$ is at medium level, the proposed ATPS approach achieves higher $\eta$ and lower $i_{pk}$ than SPS. In addition, when $P_{out}$ is low, ATPS manifests significant superiority on both $\eta$ and $i_{pk}$ compared with SPS. Furthermore, as can be seen from Fig. 24 to Fig. 26, the improvements of $\eta$ and $i_{pk}$ are more obvious when $V_2$ equals to 230 V than that when $V_2$ is 160 V.

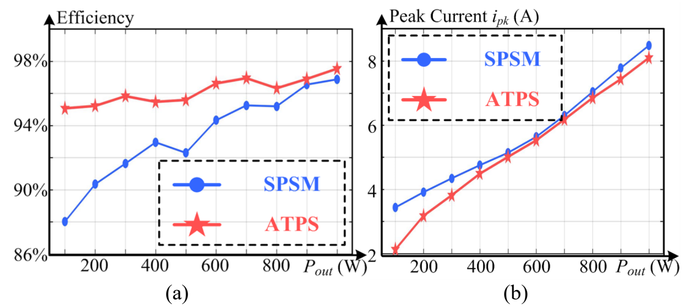


Fig. 26. $\eta$ and $i_{pk}$ of the proposed ATPS compared with SPS modulation given that $V_2$ is 230 V: (a) efficiency $\eta$; (b) current stress $i_{pk}$.

### *E. Accuracy of the Theoretical Total Power Loss via the Simulation Model in the Proposed ATPS Approach*

In this part, the theoretical analysis of total power loss via the PLECS simulation model on the optimal TPS modulations is compared with the experimental total power loss. The difference summarized in Fig. 27 proves the high accuracy of the applied PLECS model and the proposed ATPS approach.

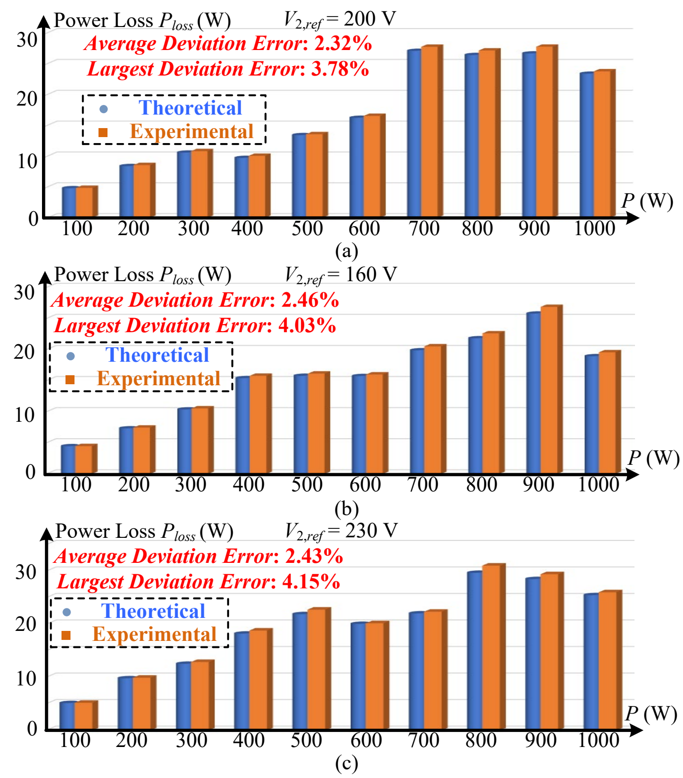


Fig.27. Deviations between theoretically analyzed total power loss via PLECS model and the experimental power loss performance for different values of output voltage: (a) $V_{2,ref}$= 200 V; (b) $V_{2,ref}$= 160 V; (c) $V_{2,ref}$= 230 V.

In specific, the deviations between theoretically analyzed power loss and experimental power loss in average are only

2.32%, 2.46% and 2.43% for output voltage $V_{2,ref}$ of values 200V, 160V and 230V, respectively. From the perspective of worst-case scenarios, in all the considered cases, the highest deviation is only 4.15%. Consequently, given the small and neglectable error between the theoretical and experimental power loss, the high accuracy of the applied simulation model as well as the proposed ATPS approach have been verified.

In a word, all the experiments in this section validate the application case in Section IV in a comprehensive manner, and the proposed ATPS for designing the efficiency-oriented optimal TPS is also empirically validated.

## VI. Conclusion

An efficiency-oriented automatic triple phase shift (ATPS) modulation has been proposed in this paper, which can realize optimal power efficiency of dual active bridge converter with a high level of automation. This proposed ATPS contains three stages. Firstly, a surrogate model is built for power loss under TPS modulation with neural network to replace traditional manual analysis and derivation. Secondly, particle swarm optimization is utilized to optimize three modulation parameters to achieve optimal power efficiency. Thirdly, fuzzy inference system is adopted to realize real-time implementation of TPS with continuous modulation performance. Through 1*k*W hardware experiments, effectiveness of ATPS modulation approach has been validated.

In the future, the optimization of the transient response time can be further studied, in which the PI parameters and hyper-parameters of fuzzy inference system can be carefully optimized.

## References

[1] P. Zumel *et al.*, ‘Modular Dual-Active Bridge Converter Architecture’, *IEEE Trans. Ind. Appl.*, vol. 52, no. 3, pp. 2444–2455, May 2016.

[2] F. Feng, X. Zhang, F. Lin, and H. B. Gooi, ‘Impedance modeling and stability analysis of dual active bridge converter with LC input filter’, *CES Trans. Electr. Mach. Syst.*, vol. 2, no. 3, pp. 289–295, Sep. 2018.

[3] F. Lin, X. Zhang, and X. Li, ‘Stability-Oriented Resonant Parameter Design for CLLC-Type Resonant Dual Active Bridge Converter with Swarm Intelligence’, in *2020 IEEE Energy Conversion Congress and Exposition (ECCE)*, Detroit, MI, USA, Oct. 2020, pp. 6175–6178.

[4] T. M. Parreiras, A. P. Machado, F. V. Amaral, G. C. Lobato, J. A. S. Brito, and B. C. Filho, ‘Forward Dual-Active-Bridge Solid-State Transformer for a SiC-Based Cascaded Multilevel Converter Cell in Solar Applications’, *IEEE Trans. Ind. Appl.*, vol. 54, no. 6, pp. 6353–6363, Nov. 2018.

[5] S. Poshtkouhi and O. Trescases, ‘Flyback Mode for Improved Low-Power Efficiency in the Dual-Active-Bridge Converter for Bidirectional PV Microinverters With Integrated Storage’, *IEEE Trans. Ind. Appl.*, vol. 51, no. 4, pp. 3316–3324, Jul. 2015.

[6] J. Sun, L. Yuan, Q. Gu, and Z. Zhao, ‘Startup Strategy With Constant Peak Transformer Current for Solid-State Transformer in Distribution Network’, *IEEE Trans. Ind. Appl.*, vol. 55, no. 2, pp. 1740–1751, Mar. 2019.

[7] L. Tarisciotti, A. Costabeber, L. Chen, A. Walker, and M. Galea, ‘Current-Fed Isolated DC/DC Converter for Future Aerospace Microgrids’, *IEEE Trans. Ind. Appl.*, vol. 55, no. 3, pp. 2823–2832, May 2019, doi: 10.1109/TIA.2018.2889845.

[8] X. Chen, G. Xu, H. Han, D. Liu, Y. Sun, and M. Su, ‘Light-load Efficiency Enhancement of High-Frequency Dual-Active-Bridge Converter Under SPS Control’, *IEEE Trans. Ind. Electron.*, pp. 1–1, 2020.

[9] L. Jin, B. Liu, and S. Duan, ‘ZVS Soft Switching Operation Range Analysis of Three-Level Dual-Active Bridge DC–DC Converter Under Phase Shift Control Strategy’, *IEEE Trans. Ind. Appl.*, vol. 55, no. 2, pp. 1963–1972, Mar. 2019.

[10] F. Wu, F. Feng, and H. B. Gooi, ‘Cooperative Triple-Phase-Shift Control for Isolated DAB DC–DC Converter to Improve Current Characteristics’, *IEEE Trans. Ind. Electron.*, vol. 66, no. 9, pp. 7022–7031, Sep. 2019.

[11] H. Shi, H. Wen, J. Chen, Y. Hu, L. Jiang, and G. Chen, ‘Minimum-Reactive-Power Scheme of Dual-Active-Bridge DC–DC Converter With Three-Level Modulated Phase-Shift Control’, *IEEE Trans. Ind. Appl.*, vol. 53, no. 6, pp. 5573–5586, Nov. 2017.

[12] D. Liu, Y. Wang, F. Deng, and Z. Chen, ‘Triple-Phase-Shift Modulation Strategy for Diode-Clamped Full-Bridge Three-Level Isolated DC/DC Converter’, *IEEE Access*, vol. 8, pp. 2750–2759, 2020.

[13] J. Lu *et al.*, ‘A Modular-Designed Three-Phase High-Efficiency High-Power-Density EV Battery Charger Using Dual/Triple-Phase-Shift Control’, *IEEE Trans. Power Electron.*, vol. 33, no. 9, pp. 8091–8100, Sep. 2018.

[14] G. Jean-Pierre, N. Altin, A. El Shafei, and A. Nasiri, ‘Efficiency Optimization of Dual Active Bridge DC– DC Converter with Triple Phase-Shift Control’, in *2020 IEEE Energy Conversion Congress and Exposition (ECCE)*, Detroit, MI, USA, Oct. 2020, pp. 1217–1222.

[15] S. Maharana, S. Mukherjee, D. De, A. Dash, and A. Castellazzi, ‘Study of Dual Active Bridge With Modified Modulation Techniques for Reduced Link Current Peak Stress and Harmonics Losses in Magnetics’, *IEEE Trans. Ind. Appl.*, vol. 56, no. 5, pp. 5035–5045, Sep. 2020.

[16] L.-C. Shih, Y.-H. Liu, and H.-J. Chiu, ‘A Novel Hybrid Mode Control for a Phase-Shift Full-Bridge Converter Featuring High Efficiency Over a Full-Load Range’, *IEEE Trans. Power Electron.*, vol. 34, no. 3, pp. 2794–2804, Mar. 2019.

[17] A. Taylor, G. Liu, H. Bai, A. Brown, P. M. Johnson, and M. McAmmond, ‘Multiple-Phase-Shift Control for a Dual Active Bridge to Secure Zero-Voltage Switching and Enhance Light-Load Performance’, *IEEE Trans. Power Electron.*, vol. 33, no. 6, pp. 4584–4588, Jun. 2018.

[18] Q. Bu, H. Wen, J. Wen, Y. Hu, and Y. Du, ‘Transient DC Bias Elimination of Dual-Active-Bridge DC–DC Converter With Improved Triple-Phase-Shift Control’, *IEEE Trans. Ind. Electron.*, vol. 67, no. 10, pp. 8587–8598, Oct. 2020.

[19] Y. A. Harrye, K. H. Ahmed, G. P. Adam, and A. A. Aboushady, ‘Comprehensive steady state analysis of bidirectional dual active bridge DC/DC converter using triple phase shift control’, in *2014 IEEE 23rd International Symposium on Industrial Electronics (ISIE)*, Istanbul, Turkey, Jun. 2014, pp. 437–442.

[20] A. Bhattacharjee, X. Chen, and I. Batarseh, ‘Analytical Solution For Minimum RMS Current and Reactive Power Modulation of A Soft Switched Dual Active Bridge Converter’, in *2019 IEEE Energy Conversion Congress and Exposition (ECCE)*, Baltimore, MD, USA, Sep. 2019, pp. 1321–1327.

[21] B. Zhao, Q. Song, W. Liu, G. Liu, and Y. Zhao, ‘Universal High-Frequency-Link Characterization and Practical Fundamental-Optimal Strategy for Dual-Active-Bridge DC-DC Converter Under PWM Plus Phase-Shift Control’, *IEEE Trans. Power Electron.*, vol. 30, no. 12, pp. 6488–6494, Dec. 2015.

[22] Cong Wang, Guanglin Sha, Hong Cheng, and Qinjia Deng, ‘Unified phasor analytical method for dual-active-bridge DC/DC converter under phase-shift control’, in *2016 IEEE 8th International Power Electronics and Motion Control Conference (IPEMC-ECCE Asia)*, Hefei, China, May 2016, pp. 348–355.

[23] Y. Shen, X. Sun, W. Li, X. Wu, and B. Wang, ‘A Modified Dual Active Bridge Converter With Hybrid Phase-Shift Control for Wide Input Voltage Range’, *IEEE Trans. Power Electron.*, pp. 1–1, 2015.

[24] L. Zhou, Y. Gao, H. Ma, and P. T. Krein, ‘Wide-load range multi-objective efficiency optimization produces closed-form control solutions for dual active bridge converter’, *IEEE Trans. Power Electron.*, pp. 1–1, 2021.

[25] F. An, W. Song, K. Yang, S. Yang, and L. Ma, ‘A Simple Power Estimation With Triple Phase-Shift Control for the Output Parallel DAB DC–DC Converters in Power Electronic Traction Transformer for Railway Locomotive Application’, *IEEE Trans. Transp. Electrification*, vol. 5, no. 1, pp. 299–310, Mar. 2019.

[26] F. Toniolo, S. Pistollato, T. Caldognetto, S. Buso, G. Spiazzi, and P. Mattavelli, ‘Implementation and Experimental Evaluation of an Efficiency-Improved Modulation Technique for IBCI DC-DC Converters’, in *2020 IEEE Applied Power Electronics Conference and Exposition (APEC)*, New Orleans, LA, USA, Mar. 2020, pp. 3430–3436.

[27] Y. Tang *et al.*, ‘RL-ANN Based Minimum-Current-Stress Scheme for the Dual Active Bridge Converter with Triple-Phase-Shift Control’, *IEEE J. Emerg. Sel. Top. Power Electron.*, pp. 1–1, 2021.

[28] H. Zhang, X. Tong, and J. Yin, ‘Optimal triple-phase-shift controller design of isolated bidirectional DC-DC converter based on ant colony algorithm and BP neural network’, in *IECON 2017 - 43rd Annual*

*Conference of the IEEE Industrial Electronics Society*, Beijing, Oct. 2017, pp. 8802–8807.

[29] H. Akagi, T. Yamagishi, N. M. L. Tan, S. Kinouchi, Y. Miyazaki, and M. Koyama, 'Power-Loss Breakdown of a 750-V 100-kW 20-kHz Bidirectional Isolated DC–DC Converter Using SiC-MOSFET/SBD Dual Modules', *IEEE Trans. Ind. Appl.*, vol. 51, no. 1, pp. 420–428, Jan. 2015.

[30] S. M. Akbar, A. Hasan, A. J. Watson, and P. Wheeler, 'Model Predictive Control with Triple Phase Shift Modulation for a Dual Active Bridge DC-DC Converter', *IEEE Access*, pp. 1–1, 2021.

[31] J. M. Cano, A. Navarro-Rodriguez, A. Suarez, and P. Garcia, 'Variable Switching Frequency Control of Distributed Resources for Improved System Efficiency', *IEEE Trans. Ind. Appl.*, vol. 54, no. 5, pp. 4612–4620, Sep. 2018.

[32] S. E. De Leon-Aldaco, H. Calleja, and J. Aguayo Alquicira, 'Metaheuristic Optimization Methods Applied to Power Converters: A Review', *IEEE Trans. Power Electron.*, vol. 30, no. 12, pp. 6791–6803, Dec. 2015.

[33] X. Li, X. Zhang, F. Lin, and F. Blaabjerg, 'Artificial-Intelligence-Based Design (AI-D) for Circuit Parameters of Power Converters', *IEEE Trans. Ind. Electron.*, pp. 1–1, 2021.

[34] J. Chrouta, W. Chakchouk, A. Zaafouri, and M. Jemli, 'Modeling and Control of an Irrigation Station Process Using Heterogeneous Cuckoo Search Algorithm and Fuzzy Logic Controller', *IEEE Trans. Ind. Appl.*, vol. 55, no. 1, pp. 976–990, Jan. 2019.

[35] C. M. Bishop, *Pattern recognition and machine learning*. New York: Springer, 2006.

[36] D. P. Kingma and J. Ba, 'Adam: A Method for Stochastic Optimization', *ArXiv14126980 Cs*, Jan. 2017, Accessed: Jul. 08, 2021. [Online]. Available: http://arxiv.org/abs/1412.6980.

**Fanfan Lin** received her bachelor degree in electrical engineering from Harbin Institute of Technology in China in 2018. From 2018, she studies as a full-time Ph. D. candidate in Nanyang Technological University in Singapore. Her research interest includes artificial intelligence application in power electronics, machine-learning-based design of power converters, dual active bridge converter, wireless power transfer, etc.

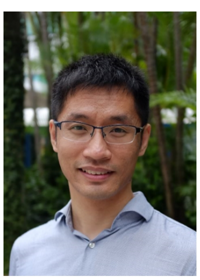

**Dr. Xin Zhang** (Senior Member, IEEE) received the Ph.D. degree in Automatic Control and Systems Engineering from the University of Sheffield, U.K., in 2016 and the Ph.D. degree in Electronic and Electrical Engineering from Nanjing University of Aeronautics & Astronautics, China, in 2014.

From February 2017 to December 2020, he was an Assistant Professor of power engineering with the School of Electrical and Electronic Engineering, Nanyang Technological University, Singapore. Currently, he is the professor at Zhejiang University. He is generally interested in power electronics, power systems, and advanced control theory, together with their applications in various sectors.

**Xinze Li** received his bachelor degree in Electrical Engineering and its Automation from Shandong University, China, 2018. He is currently a full-time Ph.D. candidate with the School of Electrical and Electronic Engineering in Nanyang Technological University, Singapore.

His research interests include artificial intelligence, machine learning, and the applications of evolutionary algorithms and deep learning in power electronics.

Dr. Changjiang Sun (S'13–M'19) received the Ph.D. degree from Shanghai Jiao Tong University, China, in 2019.

He is currently a Research Fellow with Nanyang Technological University, Singapore. His current research interests include topology and control of dc-dc converters for application in renewable energy collection and transmission grids.

**Wenjian Cai** (M'05) received the B.Eng. and M.Eng. degrees from the Department of Precision Instrumentation Engineering and the Department of Control Engineering, Harbin Institute of Technology, Harbin, China, in 1980 and 1983, respectively, and the Ph.D. degree from the Department of Electrical Engineering, Oakland University, Rochester, MI, USA, in 1992. After graduation, he was a Postdoctoral Research Fellow with the Center for Advanced Robotics, Oakland University, a Research Scientist with the National University of Singapore, Singapore, a Principal Engineer and R&D Manager with Supersymmetry Services Pte Ltd., Singapore, and a Senior Research Fellow with the Environmental Technology Institute. He is currently an Associate Professor with the Nanyang Technological University, Singapore. He has more than 20 years of industry and research experience in the areas of environmental and energy conservation technologies. He participated in many industry-related research projects and published more than 80 technical papers. His research interests include sensoring and control technologies in environmental and energy processes, multivariable control, and identification.

**Zhe Zhang** (Senior Member, IEEE) received the B.Sc. and M.Sc. degrees in power electronics from Yanshan University, Qinhuangdao, China, in 2002 and 2005, respectively, and the Ph.D. degree in electrical engineering from the Technical University of Denmark, Kongens Lyngby, Denmark, in 2010. He is currently an Associate Professor with the Department of Electrical Engineering, Technical University of Denmark (DTU). Since January 2018, he has been the Head of Studies in charge of Electrical Engineering M.Sc. Program at DTU. From 2005 to 2007, he was an Assistant Professor with Yanshan University. From June 2010 to August 2010, he was with the University of California, Irvine, CA, USA, as a Visiting Scholar. He was an Assistant Professor with the Technical University of Denmark, from 2011 to 2014. He has authored or co-authored more than 150 transactions and international conference papers and filed over ten patent applications. He has supervised more than ten Ph.D. students since 2013. His current research interests include applications of wide bandgap devices, high frequency dc–dc converters, multiple-input dc–dc converters, soft switching power converters, and multilevel dc–ac inverters for renewable energy systems, hybrid electric vehicles and uninterruptable power supplies; piezoelectric-actuator and piezoelectric-transformer based power conversion systems. Dr. Zhang was the recipient of several awards and honors including Best Paper Awards in IEEE ECCE 2016, IEEE IGBSG 2018, IEEE IFEEC 2019, IEEE ECCE Asia 2020, Best Teacher of the Semester, Chinese Government Award for Outstanding Students Abroad, etc. He is also an Associate Editor for IEEE TRANSACTIONS ON INDUSTRIAL ELECTRONICS, Associate Editor for IEEE JOURNAL OF EMERGING AND SELECTED TOPICS IN POWER ELECTRONICS, Associate Editor for IEEE ACCESS, and Guest Editor for IEEE JOURNAL OF EMERGING AND SELECTED TOPICS IN INDUSTRIAL ELECTRONICS.